Interannual variations in the Atlantic meridional overturning circulation and its relationship with the net northward heat transport in the South Atlantic

Shenfu Dong,[1] Silvia Garzoli,[2] Molly Baringer,[2] Christopher Meinen,[2] and Gustavo Goni[2]

[1] Variability of the Atlantic Meridional Overturning Circulation (AMOC) and its effect on the net northward heat transport (NHT) in the South Atlantic are examined using a trans-basin expendable bathythermograph (XBT) high-density line at 35°S (AX18). The time-mean AMOC is 17.9 ± 2.2 Sv during 2002–2007. Although the geostrophic transport dominates the time-mean AMOC, both geostrophic and Ekman transports are important in explaining the AMOC variability. The contributions of geostrophic and Ekman transports to the AMOC show annual cycles, but they are out of phase, resulting in weak seasonal variability of the AMOC. The NHT variability is significantly correlated with the AMOC, where a 1 Sv increase in the AMOC would yield a 0.05 ± 0.01 PW increase in the NHT. Partition of transport into the western and eastern boundaries and interior suggests that, to quantify changes in the AMOC and NHT, it is critical to monitor all three regions. **Citation:** Dong, S., S. Garzoli, M. Baringer, C. Meinen, and G. Goni (2009), Interannual variations in the Atlantic meridional overturning circulation and its relationship with the net northward heat transport in the South Atlantic, *Geophys. Res. Lett.*, *36*, L20606, doi:10.1029/2009GL039356.

1. Introduction

[2] In recent years great interest has been aroused in monitoring the AMOC due to its link to the past abrupt climate change and anthropogenic climate forcing [e.g., *Broecker*, 1997]. Majority of the AMOC observations have been focused on the North Atlantic. Hydrographic observations in the South Atlantic have been historically fewer, which has hampered efforts to understand the South Atlantic impacts on the AMOC. However, the South Atlantic is particularly important as a region where oceanic properties are exchanged, mixed, and redistributed between different ocean basins, and it is unique as the only major ocean basin that transports heat from the poles towards the equator [*Talley*, 2003]. Model studies [e.g., *Weijer et al.*, 2002] suggested that the inter-ocean exchanges in the South Atlantic can significantly alter long-term MOC response.

[3] As part of the NOAA contribution to the Global Ocean Observing System, a zonal XBT transect (AX18) was started in 2002 in the South Atlantic (~35°S) between Cape Town, South Africa and Buenos Aires, Argentina (Figure 1a). One of the main objectives of this transect is to monitor the upper limb of the MOC as it enters the Atlantic, providing the first critical 'time series' observations in this region. The AX18 transect was sampled twice per year in 2002 and 2003. Since 2004 AX18 has been carried out four times per year. Due to ship availability, the AX18 line carried out after March 2007 were conducted on an alternate track between Cape Town and Santos, Brazil, moving the western end of the transect up to 25°S. Readers are referred to *Baringer and Garzoli* [2007] for detailed description of AX18 and the methodology of computing the net northward heat transports (NHT) from the trans-basin XBT line.

[4] *Garzoli and Baringer* [2007] analyzed the NHT from the first 14 AX18 transects. In this study the AMOC variability from the AX18 and its relationship with the NHT are examined. Contributions of the geostrophic and Ekman transports to the AMOC, as well as those from the boundary currents and interior flow are quantified. Although initial sensitivity studies indicate that the results are not particularly dependent on the northward shift of the AX18 line, the present study is focused on the 17 transects prior to the movement of the western endpoint between July 2002 and March 2007.

2. AMOC Variability Across 35°S

[5] A brief review of the methodology of *Baringer and Garzoli* [2007] for estimating transports across AX18 line is provided here. Salinity profiles are estimated for each XBT profile by using historical temperature/salinity relationship for each location and depth. Temperature/salinity profiles are then extended to the ocean bottom using the World Ocean Atlas 2005 climatology. Transports are calculated in 76 vertical layers, with 20 m layer thickness in the upper 1000 m and 200 m thick layers below 1000 m. The initial level of no motion was chosen at $\sigma_2 = 37.09$ kgm^{-3} (σ_2 defined as potential density relative to 2000 dbar minus 1000 kgm^{-3}), at ~3700 m depth where the upper overturning limb is separated from the lower overturning limb. This level of no motion is then uniformly adjusted so that the net salt transport across the section matches the salt flux through the Bering Straits (26.7 × 10^6 kg s^{-1} [*Coachman and Aagaard*, 1988]). This salt flux constraint results in an average southward volume flux of 0.5 Sv, and a corresponding southward temperature flux of 0.009 PW, much smaller than the NHT. This methodology assumes that the non-Ekman ageostrophic transports, such as inertial motions and eddy fluxes, are small, which has been confirmed through analyzing numerical model outputs [*Baringer and Garzoli*, 2007]. Details of error estimates from various sources (rings, reference velocity) are given by *Baringer and Garzoli* [2007].

[6] An example of the meridional velocity distribution for the December 2004 transect is shown in Figure 1b. The zonal

[1]CIMAS, University of Miami, Miami, Florida, USA.
[2]AOML, NOAA, Miami, Florida, USA.
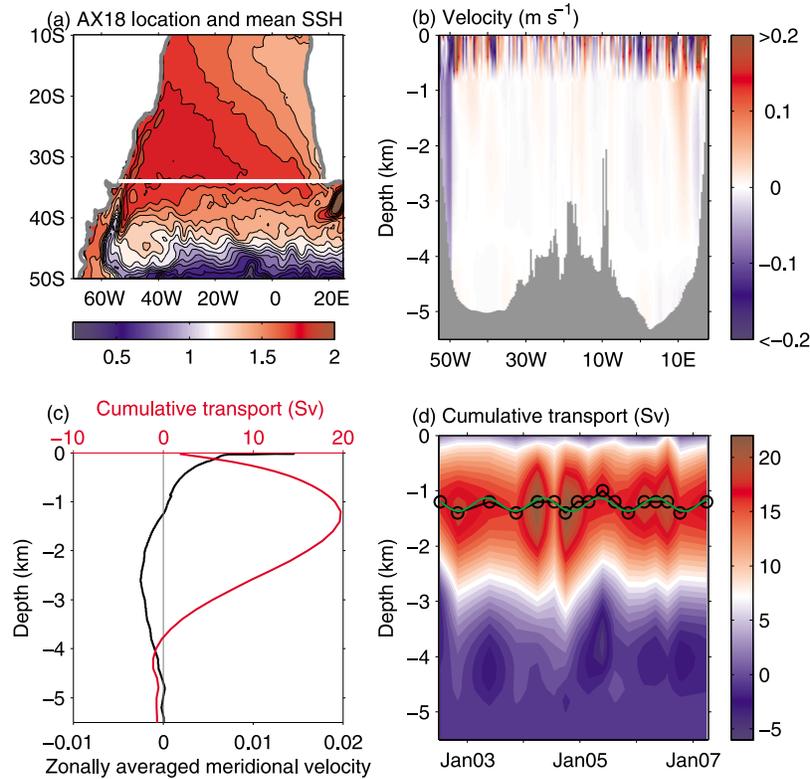
Figure 1. (a) Mean sea surface height illustrating the mean gyre orientation. The white line approximates the AX18 location. (b) Meridional velocity distribution along AX18 for the December 2004 transect. (c) Vertical distribution of the zonally averaged meridional velocity (black, bottom axis), and cumulative volume transport from the surface to ocean bottom (red, top axis). (d) The cumulative volume transport for all 17 AX18 transects. Black circles indicate the depth at which the cumulative transport reaches the maximum, and the green line is the annual harmonic of this depth.

structure of the velocity is dominated by mesoscale structures in the upper ocean. A major feature of the velocity is the strong southward flow near the western boundary associated with the contribution of the Deep Western Boundary Current and the Brazil Current. The zonally averaged velocity shows a simplified vertical structure (Figure 1c), with northward flow in the upper 1200 m and southward flow in the lower water column. The cumulative volume transport from the surface to the ocean bottom increases with depth from the surface to about 1200 m; it then decreases with depth to the ocean bottom. The depth of the maximum cumulative transport indicates where the meridional transport reverses direction from northward in the upper layer to southward in the lower layer. Hence, the maximum cumulative transport represents the total northward transport in upper water column, and is defined here as the strength of AMOC. In general, the maximum cumulative transport is found between 1000–1400 m depth (Figure 1d). The average depth from those 17 occupations is ∼1250 m, slightly deeper than the 1100 m found in the North Atlantic from the first year RAPID/MOCHA array [*Cunningham et al.*, 2007]. The depth of the maximum cumulative transport exhibits an annual cycle (Figure 1d), with the shallowest depth of 1130 m in May and the deepest depth of 1370 m in November.

[7] The AMOC from the 17 occupations varies from 13.8 Sv (July 2004) to 22.0 Sv (March 2004) with an average of 17.9 Sv and a standard deviation of 2.2 Sv (Figure 2a). Of this 17.9 Sv transport, 15.9 Sv comes from upper 800 m, suggesting that 89% of the AMOC is captured by XBT

measurements. The mean value is comparable with the annual mean AMOC of 18.7 Sv observed from the first year RAPID/MOCHA array at 26.5°N [*Cunningham et al.*, 2007]. Similar values of the AMOC in the North and South Atlantic have been suggested by *Talley* [2003] using the hydrographic section measurements. The geostrophic and Ekman transports above the depth of the maximum cumulative transport were separated to determine their relative contributions to the AMOC. The Ekman transport is estimated using monthly wind stress from the NCEP/NCAR Reanalysis. About 88% (15.7 ± 2.6 Sv) of the time-mean AMOC is contributed by the geostrophic transport (Figure 2a). Although the northward Ekman transport is only 2.2 Sv on average, its variability is comparable with that of the AMOC. The variance of the AMOC, and its geostrophic and Ekman components are 4.7 Sv^2, 6.8 Sv^2 and 4.0 Sv^2, respectively, suggesting that in the South Atlantic measurements of both geostrophic and Ekman transports are critical for the determination of AMOC variability.

[8] To examine the relative contributions of boundary currents to the AMOC, we separate the volume transport into three regions: the western boundary (west of where current changes from southward to northward, ∼48°W), the eastern boundary (east of the western edge of the Walvis Ridge, ∼3°E), and interior (48°W–3°E). Figure 2b shows the west-to-east cumulative transport averaged for all 17 sections, and illustrates the regional separation. The results presented here are not particularly sensitive to these definitions as long as the boundaries are offshore of the boundary currents
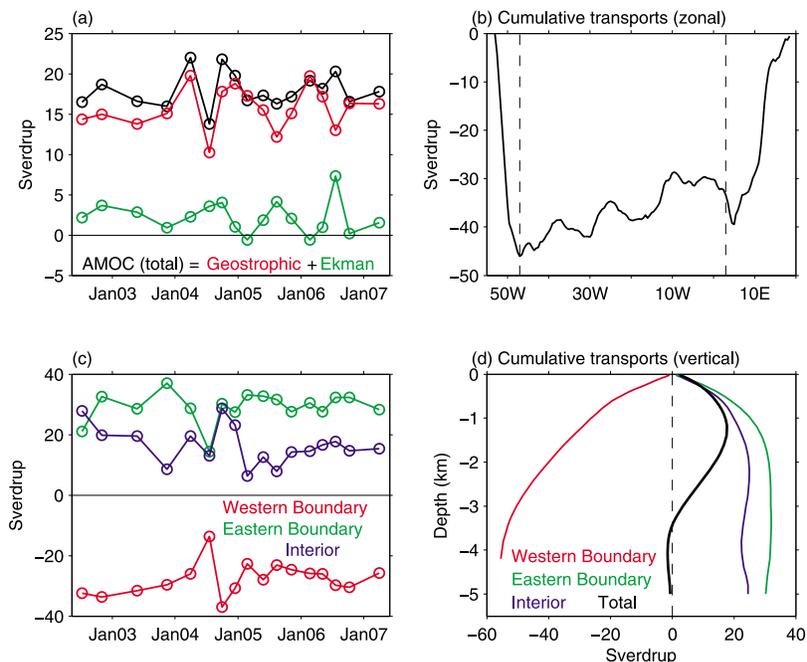
Figure 2. (a) Time series of the AMOC (black) and contributions from the geostrophic (red) and Ekman (green) components. (b) West-to-East cumulative transports (in Sv) averaged over the 17 AX18 transects. The dashed lines indicate the separation points for the boundary currents and interior. (c) Contributions of the western (red) and eastern (green) boundaries and interior (blue) to the AMOC. (d) The total cumulative volume transport (black) from the surface to ocean bottom, and those in the western (red) and eastern (green) boundaries and interior (blue) for the December 2004 transect.

themselves. The transport in each region is integrated from surface to the depth of the maximum cumulative transport (Figure 1d). The eastern boundary (Figure 2c) shows a strong northward transport related to the Benguela Current, with an average of 29.2 ± 5.2 Sv, which agrees with the eastern boundary transport of 30 Sv from historical hydrographic data [*Stramma and Peterson*, 1989]. The averaged southward transport in the western boundary (−27.7 ± 5.3 Sv, Figure 2c) is larger than those from previous studies of around 20 Sv (see *Peterson and Stramma* [1991] for a detailed summary), this lower value may be due to the shallower reference depth normally used in past studies. The northward transport in the interior (16.5 ± 6.3 Sv) is about half of that in the eastern boundary (Figure 2c), but its variability is the largest among the three regions. The importance of the boundary currents in AMOC variability have been emphasized in various studies [e.g., *Biastoch et al.*, 2008], whereas the strong time-variability in the interior suggests that it is also important to monitor interior flow in order to quantify variability in the AMOC. Statistical analysis suggests that the AMOC variability has the highest correlation with that in the interior, which also highlights the importance of the interior flow.

[9] Examination of the cumulative volume transport in each region (Figure 2d) indicates that the volume transports in the eastern boundary and interior regions are confined in the upper 1500 m. In contrast, in the western boundary the deep ocean contributes a significant amount to the total volume transport: the layer between 1500 m and the ocean bottom contributes about 40% of the total meridional transport. An example of the cumulative transports shown in Figure 2d clearly illustrates why it is important to monitor the whole water column in order to capture the vertical

structure of the volume transport, and hence to define the strength of the AMOC.

3. Seasonal Variations in the AMOC

[10] An annual harmonic analysis of the AMOC indicates that the peak-to-peak amplitude of its seasonal signal is about 1.8 Sv. However, this seasonal signal is statistically insignificant (Figure 3a), suggesting that the AMOC variability is not dominated by seasonal cycle. In contrast to the AMOC, both geostrophic and Ekman contributions experience strong and statistically significant seasonal cycles (Figures 3b and 3c). The amplitude of the seasonal cycle in geostrophic transport is 6.1 Sv, with its maximum in August and minimum in February. The seasonal cycle of Ekman transport has an amplitude of 4.2 Sv. The Ekman and geostrophic transports are 180° out of phase, resulting in a weak seasonal signal for the AMOC. The seasonal signal in geostrophic and Ekman transports explains 61% and 51% of their total variance, respectively. These seasonal characteristics of the AMOC and contributions from geostrophic and Ekman components are similar to those of the NHT [*Garzoli and Baringer*, 2007].

[11] The peak-to-peak amplitudes of seasonal variations in the regional contributions to the AMOC are 4.3 Sv, 6.3 Sv, and 3.7 Sv for the western and eastern boundaries and the interior, respectively (Figure 3d). However, only in the eastern boundary the seasonal cycle is statistically significant, where the transport is dominated by the geostrophic component.

[12] To demonstrate the effects of wind forcing on the seasonal variability in geostrophic and Ekman contributions to the AMOC, Figures 3e and 3f show the long-term mean
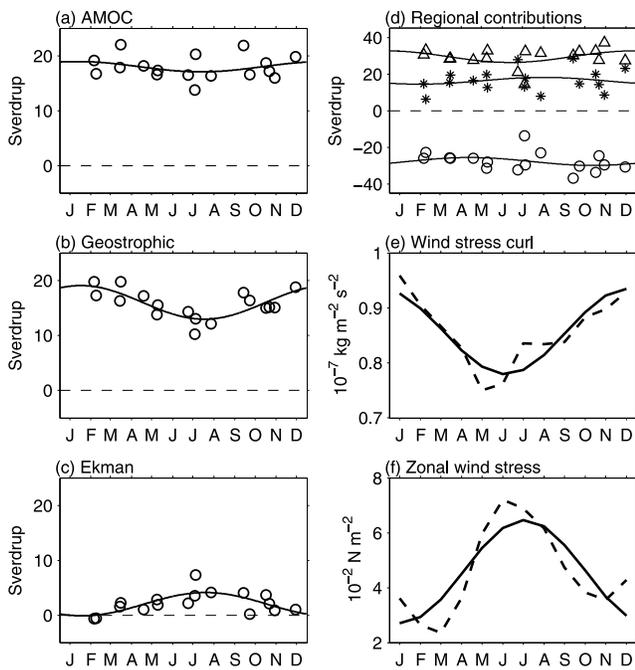
Figure 3. Scatter plots of the (a) AMOC, and its (b) geostrophic and (c) Ekman contributions versus month. (d) Contributions of the western (circles) and eastern (triangles) boundaries and the interior (stars) to the AMOC. The black lines show the annual cycle. Monthly (e) climatological (dashed) wind stress curl and (f) zonal wind stress averaged in the subtropical south Atlantic (box indicated in Figure 3d). Solid lines in Figures 3e and 3f are the corresponding annual harmonic.

wind stress curl and zonal wind stress averaged over the subtropical South Atlantic. The seasonal variation in geostrophic transport is correlated with the seasonal signal of wind stress curl (Figure 3e). It is no surprise that the seasonality of the northward Ekman transport (Figure 3c) is highly coherent with that of the zonal wind stress (Figure 3f), which is strong in winter and weak in summer.

4. Relationship Between AMOC Strength and Northward Heat Transport

[13] *Garzoli and Baringer* [2007] have reported the NHT from the first 14 AX18 transects, which gave a mean value of 0.54 ± 0.11 PW. The average of the NHT from the 17 transects gives a similar value of 0.55 ± 0.14 PW. The heat transports (Figure 4) estimated from the 17 transects vary from 0.28 PW (October 2006) to 0.82 PW (December 2004), which is well within the range of estimates from previous studies (e.g., -0.24 to 0.6 PW across $30°$S from *de las Heras and Schlitzer* [1999] and 0.45 to 0.94 PW from *Saunders and King* [1995]). Here the relationship of NHT with the AMOC strength is examined for those 17 transects. The contributions of boundary currents and interior flow to the NHT are also evaluated, which was not examined in earlier analysis of *Garzoli and Baringer* [2007].

[14] The variability in NHT correlates well (r = 0.76, exceeding the 95% significance level of 0.47) with that in the AMOC strength (Figure 4a). The positive correlation suggests that a large NHT corresponds to a strong AMOC,

consistent with model results [*Danabasoglu*, 2008]. Regressing the NHT to the AMOC indicates that 1 Sv increase in the AMOC would increase the NHT by 0.05 ± 0.01 PW. There are no significant changes in the correlation-regression analyses after removing seasonal cycles from the AMOC and NHT.

[15] To examine the contributions of various regions to the NHT, the heat transports are separated into the same three regions as the volume transport: the eastern and western boundaries, and interior. The eastern boundary is the major contributor to the NHT with an average of 1.33 ± 0.27 PW. The northward transport from the interior is 0.80 ± 0.35 PW, just over half of the mean in the eastern boundary and it has a larger standard deviation. In the western boundary the southward heat transport is -1.59 ± 0.33 PW. It is important to note that the time-variability of the three regions are of comparable magnitude, illustrating the critical need for monitoring all three regions in order to quantify variability in the total NHT at $35°$S.

[16] As discussed by *Garzoli and Baringer* [2007], the seasonal signal in the NHT is weak because of the compensation of the geostrophic and Ekman transports. The northward transport is slightly weaker during austral winter than that during austral summer. Similar to the AMOC strength, as we separate the NHT into three regions (western and eastern boundaries, and interior), no seasonal signal is shown in the western boundary and interior. The seasonality of heat transport in the eastern boundary is also marginal (not shown).
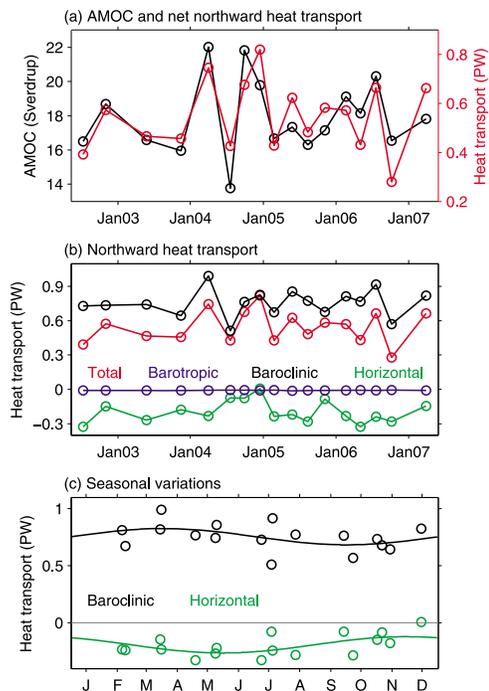
Figure 4. Time series of (a) the NHT (red, right axis) and the AMOC (black, left axis), and (b) the NHT (red) and contributions from the barotropic (blue), overturning (black), and horizontal (green) components. (c) Scatter plots of the overturning (black) and horizontal (green) heat fluxes versus month. Units are PW for heat transports and Sv for volume transports.

[17]   The NHT can be divided into three components: the barotropic, baroclinic (overturning), and the horizontal heat fluxes following *Bryden and Imawaki* [2001]. Readers are directed to *Bryden and Imawaki* [2001] for detailed description of the methodology. The barotropic temperature fluxes are small with an average value of 0.009 PW (Figure 4b). The overturning heat flux explains 70% of the NHT variability. The mean northward overturning heat flux is about 0.75 ± 0.12 PW. The horizontal heat flux is southward with a mean value of -0.20 ± 0.10 PW. An examination of the seasonal cycle in the heat fluxes indicates that both the overturning and horizontal components have a seasonal cycle of 0.14 PW, but they are about 4 months out of phase (Figure 4c), which again, explains the lack of seasonality in the NHT.

5.   Summary and Conclusions

[18]   The mean AMOC at 35°S in the South Atlantic is 17.9 ± 2.2 Sv during 2002–2007. About 88% of the mean AMOC is contributed by the geostrophic transport. However, both the geostrophic and Ekman transports are important in explaining the AMOC variability. The contributions of geostrophic and Ekman transports to the AMOC show annual cycles, but they are out of phase, resulting in weak seasonal variability in the AMOC. Examination of the contributions from boundary currents and interior indicates that transport variability of all three regions is comparable, suggesting the importance to monitor all three regions in order to quantify changes in the AMOC. The variability of the NHT at 35°S is significantly correlated with the AMOC strength, a 1 Sv increase in the AMOC would yield a 0.05 ± 0.01 PW increase in the NHT. Thus a 5–6% change in the AMOC results in a 10% change in the NHT, clearly illustrating the climatic importance of accurately monitoring the AMOC. Separation of the NHT into the overturning and horizontal heat fluxes indicates that the bulk of the NHT is associated with the overturning component.

References

Baringer, O. M., and S. L. Garzoli (2007), Meridional heat transport determined with expendable bathythermographs. Part I: Error estimates from model and hydrographic data, *Deep Sea Res., Part I, 54*, 1390–1401, doi:10.1016/j.dsr.2007.03.011.

Biastoch, A., C. W. Boning, and J. R. E. Lutjeharms (2008), Agulhas leakage dynamics affects decadal variability in Atlantic overturning circulation, *Nature, 456*, 489–492, doi:10.1038/nature07426.

Broecker, W. S. (1997), Thermohaline circulation, the Achilles heel of our climate system: Will man-made CO_2 upset the current balance?, *Science, 278*, 1582–1588, doi:10.1126/science.278.5343.1582.

Bryden, H. L., and S. Imawaki (2001), Ocean heat transport, in *Ocean Circulation and Climate, Int. Geophys. Ser.*, vol. 77, edited by G. Siedler, J. Church, and J. Gould, pp. 455–474, Academic, San Diego, Calif.

Coachman, L. K., and K. Aagaard (1988), Transports through Bering Strait: Annual and interannual variability, *J. Geophys. Res., 93*, 15,535–15,539, doi:10.1029/JC093iC12p15535.

Cunningham, S. A., et al. (2007), Temporal variability of the Atlantic meridional overturning circulation at 26.5°N, *Science, 317*, 935–938, doi:10.1126/science.1141304.

Danabasoglu, G. (2008), On multidecadal variability of the Atlantic meridional overturning circulation in the Community Climate System Model version 3, *J. Clim., 21*, 5524–5544, doi:10.1175/2008JCLI2019.1.

de las Heras, M. M., and R. Schlitzer (1999), On the importance of intermediate water flows for the global ocean overturning, *J. Geophys. Res., 104*, 15,515–15,536, doi:10.1029/1999JC900102.

Garzoli, S., and M. O. Baringer (2007), Meridional heat transport determined with expandable bathythermographs—Part II: South Atlantic transport, *Deep Sea Res., Part I, 54*, 1402–1420, doi:10.1016/j.dsr.2007.04.013.

Peterson, R. G., and L. Stramma (1991), Upper-level circulation in the South Atlantic Ocean, *Prog. Oceanogr., 26*, 1–73, doi:10.1016/0079-6611(91)90006-8.

Saunders, P. M., and B. A. King (1995), Oceanic fluxes on the WOCE A11 section, *J. Phys. Oceanogr., 25*, 1942–1958, doi:10.1175/1520-0485(1995)025<1942:OFOTWA>2.0.CO;2.

Stramma, L., and R. G. Peterson (1989), Geostrophic transport in the Benguela Current region, *J. Phys. Oceanogr., 19*, 1440–1448, doi:10.1175/1520-0485(1989)019<1440:GTITBC>2.0.CO;2.

Talley, L. D. (2003), Shallow, intermediate, and deep overturning components of the global heat budget, *J. Phys. Oceanogr., 33*, 530–560, doi:10.1175/1520-0485(2003)033<0530:SIADOC>2.0.CO;2.

Weijer, W., W. P. M. de Ruijter, A. Sterl, and S. S. Drijfhout (2002), Response of the Atlantic overturning circulation to South Atlantic sources of buoyancy, *Global Planet. Change, 34*, 293–311, doi:10.1016/S0921-8181(02)00121-2.

———————————

M. Baringer, S. Garzoli, G. Goni, and C. Meinen, AOML, NOAA, 4301 Rickenbacker Cswy., Miami, FL 33149, USA.

S. Dong, CIMAS, University of Miami, 4600 Rickenbacker Cswy., Miami, FL 33149, USA. (shenfu.dong@noaa.gov)